ACS Medicinal Chemistry Letters

Letter

pubs.acs.org/acsmedchemlett

Novel ^{64}Cu-Labeled CUDC-101 for in Vivo PET Imaging of Histone Deacetylases

Qingqing Meng,[†] Feng Li,[†] Sheng Jiang,[‡] and Zheng Li*[,†]

[†]Department of Translational Imaging, The Methodist Hospital Research Institute, Houston, Texas 77030, United States

[‡]Laboratory of Medicinal Chemistry, Guangzhou Institute of Biomedicine and Health, Chinese Academy of Sciences, Guangzhou 510530, China

Supporting Information

ABSTRACT: We report the design, synthesis, and biological evaluation of a ^{64}Cu-labeled histone deacetylase (HDAC) imaging probe, which was obtained by introduction of metal chelator through click reaction of HDAC inhibitor CUDC-101 and then radiolabeled with ^{64}Cu. The resulting ^{64}Cu-labeled compound 7 ([^{64}Cu]7) was identified as a positron emission tomography (PET) imaging probe to noninvasively visualize HDAC expression in vivo. Cell based competitive assay established the specific binding of [^{64}Cu]7 to HDACs. Biodistribution and small-animal microPET/CT studies further showed that [^{64}Cu]7 had high tumor to background ratio in the MDA-MB-231 xenograft model, a triple-negative breast cancer with high expression of HDACs. To our knowledge, [^{64}Cu]7 thus represents the first ^{64}Cu-labeled PET HDAC imaging probe, which exhibits nanomolar range binding affinity and capability to imaging HDAC expression in triple-negative breast cancer in vivo.

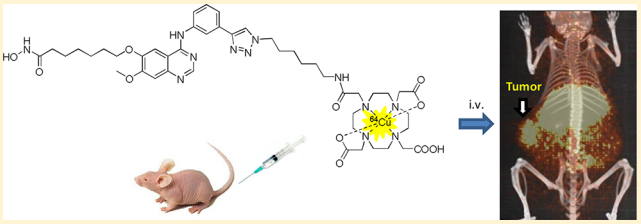

KEYWORDS: *PET imaging probe, ^{64}Cu radiolabeling, histone deacetylases inhibitors, CUDC-101, triple-negative breast cancer*

Histone deacetylases (HDACs) are a class of enzymes modulating gene expression via deacetylation of both histone and nonhistone proteins, and thereby, these enzymes are involved in a wide range of biological processes.[1−3] Many HDAC inhibitors have shown excellent properties for tumor therapy in clinical trials. To date, 18 mammalian HDAC subtypes have been discovered and accordingly classified into four classes based upon their phylogeny.[4,5] Class I (HDACs 1−3 and 8), class IIa HDACs (4, 5, 7, and 9), class IIb HDACs (6 and 10), and the class IV (11) are Zn-dependent hydrolases, whereas class III (sirtuins 1−7) enzymes are NAD$^+$-dependent Sir2-like deacetylases.[5] Class I HDACs are mostly localized within the nucleus, whereas class II HDACs shuttle between nucleus and cytoplasm. HDAC isoforms are highly expressed in various cancers, including breast cancer, pancreatic cancer, colorectal cancer, prostate cancer, and hepatocellular carcinoma.[6−8] Treatment of tumor cells with HDAC inhibitors results in growth arrest, differentiation, and apoptosis, promoting these enzymes as potential cancer drug targets.[9,10]

HDAC inhibitors (HDACi) are divided into several structural classes including hydroxamates, cyclic peptides, aliphatic acids, and benzamides.[11] So far, more than 11 new HDACi are in various stages of clinical development for therapy of multiple cancer types.[12] Among them, suberoylanilide hydroxamic acid (SAHA, Vorinostat, Merck Research Laboratories) and FK228 (Romidepsin, Celgene)[2] have been approved by US FDA for the treatment of cutaneous T-cell lymphoma. To evaluate the efficiency of existing and novel HDACi and acquire important basic scientific insight of biological and molecular events of HDACs, there is an increasing need for HDAC targeting imaging probes. To date, limited noninvasive HDAC imaging probes were reported for cancer diagnosis and therapy evaluation of HDACi in vivo.[13] For example, in Figure 1, [^{18}F]fluoroacetamide-1-hexanoicanilide (FAHA) and [^{11}C]MS-275 were reported for brain cerebral HDAC imaging.[14,15] ^{18}F-suberoylanilide hydroxamic acid (^{18}F-SAHA) was reported to be able to evaluate the target efficacy of HDAC inhibitor SAHA within 24 h of drug administration in a murine ovarian cancer model.[16]

Breast cancer is one of the leading causes of cancer death in women. Recent studies found that HDACs were correlated with estrogen receptor (ER) and progesterone receptor (PR) expression, and its expression enabled a more precise assessment of the prognosis of breast cancer patients.[17,18] Introducing HDACi in breast cancer treatment could overcome resistance to hormonal therapy.[19] HDACi was also reported to selectively target triple-negative breast cancer cell proliferation and survival in vitro and tumorigenesis in vivo.[20] HDACs as a promising biomarker play an increasingly important role in breast cancer treatment. For breast cancer imaging, targeted ER and human epidermal growth factor receptor 2 (HER2) imaging probe is currently under intense preclinical and clinical investigation; however, these agents only apply to ER or HER2-positive subtypes.[21] Imaging probes targeting other major

Received: May 17, 2013
Accepted: July 25, 2013
Published: July 25, 2013

ACS Publications © 2013 American Chemical Society

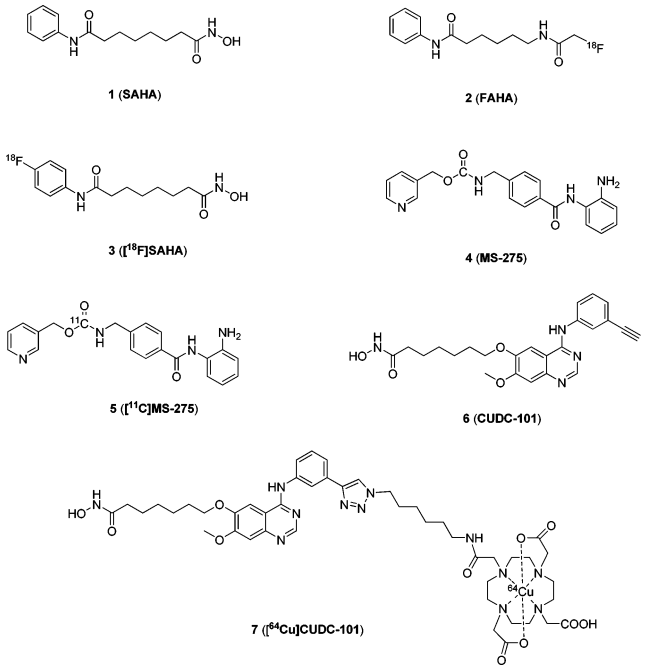

Figure 1. Chemical structures of representative HDAC inhibitors and HDAC PET imaging probes.

cellular receptors or biomarkers like HDACs are highly in demand for breast cancer diagnosis and therapy evaluation especially for triple-negative subtype patients who usually have poor prognosis. Herein, to our best of knowledge, we report the first ^{64}Cu-labeled ($t_{1/2}$ = 12.7 h; β^+ 655 keV, 17.8%) HDAC PET imaging probe [^{64}Cu]7 developed from a HDACi, 7-(4-(3-ethynylphenylamino)-7-methoxyquinazolin-6-yloxy)-*N*-hydroxyheptanamide (CUDC-101, Selleckchem, TX), which is currently in phase I clinical trials with multiple tumor types including advanced breast cancer.[22,23]

As a member of hydroxamates HDACi, CUDC-101 has the distinguishing characteristics including a hydroxamic acid group interacting with zinc at the active site of HDACs to interfere with enzyme activity, carbon linker, and capping group.[24] The capping group is solvent-exposed and interacts with amino acids near the entrance of the active site.[25,26] In this study, chelator 1,4,7,10-tetraazacyclododecane-1,4,7,10-tetraacetic acid (DOTA, Macrocyclics, TX) was conjugated to CUDC-101 with a hydrophobic carbon chain linker by click reaction. Our synthesis started from commercially available CUDC-101, which was then reacted with a carbon chain linker bearing an azide group at one end as well as a primary amine group at the other end. After the introduction of the linker, compound **9** was conjugated to DOTA-NHS in the presence of NEt_3 to give compound 7 (Scheme 1) (Supporting Information).

We subsequently determined HDAC binding activity of compound 7 using the Fluor-de-Lys HDAC Fluorimetric Assay/Drug Discovery Kit (Enzo Life Sciences, NY). The IC_{50} value of 7 was measured as 94.47 ± 19.24 nM (Supporting Information Figure S1). This finding thus identified 7 as a promising candidate for the development of ^{64}Cu HDAC targeting PET imaging probe. Compound 7 was radiolabeled by incubating with $^{64}CuCl_2$ (Washington University, MO) in 0.1 N NaOAc buffer (pH 5.5) at 60 °C for 1 h (Scheme 1). The labeled product [^{64}Cu]7 was then directly purified by radio-HPLC with ≥98% radiochemical yield and chemical purity. The specific activity of [^{64}Cu]7 was estimated to 2.5−3.0 GBq/mg (2.4−2.9 MBq/nmol) at the end of synthesis. [^{64}Cu]7 was stable in Dulbecco's modified Eagle's medium (DMEM) containing 10% fetal bovine serum (FBS) for up to 24 h at 37 °C (Supporting Information).

Scheme 1. Radiosynthesis of [^{64}Cu]7[a]

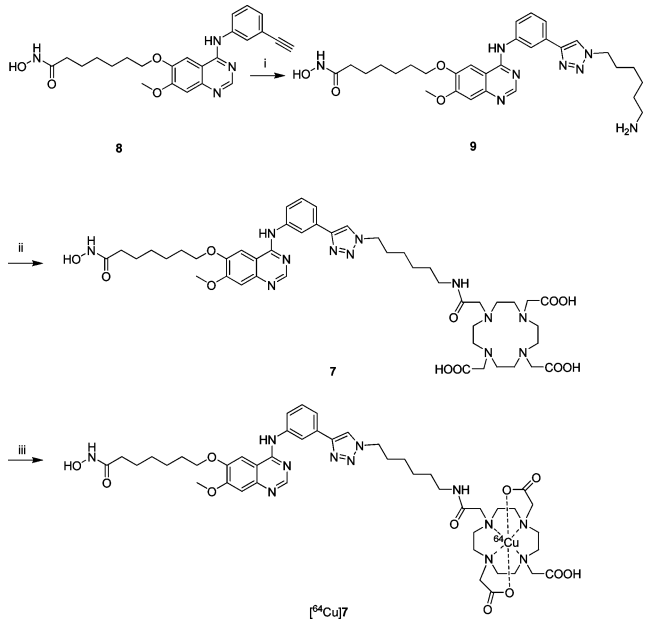

[a]Reagents and conditions: (i) 6-azidohexan-1-amine, sodium ascorbate, $CuSO_4$, H_2O/*t*-BuOH, r.t., 24 h. (ii) DOTA−NHS, NEt_3, DMSO. (iii) $^{64}CuCl_2$, 0.1 M NH_4OAc (pH = 5.5), 60 °C, 1 h.

To determine the HDAC specificity of [^{64}Cu]7, a competitive cell binding assay was performed by competition of [^{64}Cu]7 with increasing concentration of HDAC inhibitor CUDC-101 using MDA-MB-231, a triple-negative human breast cancer cell line with high HDACs expression.[27] The cellular retention and internalization of radioactivity was determined using a γ counter (Perkin-Elmer Packard, CT). The results showed that the cell uptake of [^{64}Cu]7 decreased along with the increasing of the CUDC-101 concentration, which provided evidence for target-mediated binding to HDAC-expressing cells (Figure 2). This competitive cell binding assay that established the cell uptake of [^{64}Cu]7 was realized by its specific binding to HDAC in vitro.

The in vivo imaging of mice bearing human triple-negative breast cancer MDA-MB-231 xenograft tumors was carried out

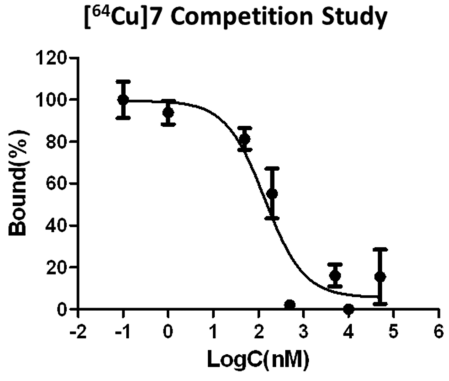

Figure 2. In vitro dose−response profile for [^{64}Cu]7 competition with CUDC-101 on the MDA-MB-231 breast cancer cells.

dx.doi.org/10.1021/ml400191z | *ACS Med. Chem. Lett.* 2013, 4, 858−862

by static microPET/CT scans at 2, 6, and 24 h after tail-vein injection of [^{64}Cu]7 (100 μCi, 3.7 MBq) (n = 4). Representative coronal slices with tumor are shown in Figure 3a. The radioactive uptake in the PET images was expressed as

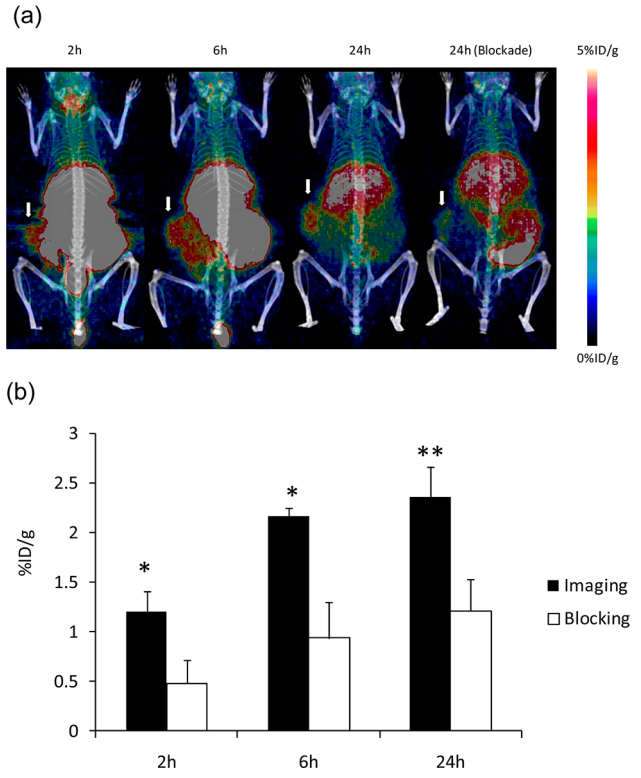

Figure 3. (a) Decay-corrected microPET/CT scan of MDA-MB-231 tumor bearing mice (n = 4) at 2, 4, and 24 h after i.v. injection of [^{64}Cu]7. The image obtained with coinjection of CUDC-101 (20 mg/kg body weight) is shown for a 24 h blockade (right). Tumors are indicated by arrows. (b) Decay-corrected region-of interest (ROI) analysis on microPET images of the tumor uptake of [^{64}Cu]7 with or without coinjection of CUDC-101 (20 mg/kg body weight). *, P < 0.05; **, P < 0.01.

a percentage of the injected radioactive dose per gram of tissue (%ID/g). From the PET imaging, the tumor was clearly visible as early as 2 h postinjection (p.i.). [^{64}Cu]7 had the high uptake in the liver, kidney, and tumor, with relatively low distribution in other tissues at 24 h p.i. Region-of-interest (ROI) analysis on microPET images showed that the tumor uptake values were 1.20 ± 0.21, 2.16 ± 0.08, and 2.36 ± 0.31% ID/g at 2, 6, and 24 h p.i., respectively (Figure 3b). To test the HDAC specificity of [^{64}Cu]7 in vivo, blocking experiments were performed by coinjection of 20 mg/kg nonradioactive HDAC inhibitor CUDC-101 with [^{64}Cu]7 . The MDA-MB-231 tumor uptake values for blocking experiments were 0.48 ± 0.24, 0.94 ± 0.37, and 1.22 ± 0.31% ID/g at 2, 6, and 24 h p.i., respectively, which showed significant decreasing compared with that of the imaging group at all time points (Figure 3b). In the blood clearance study shown in Figure S2 (Supporting Information), [^{64}Cu]7 was rapidly cleared from the blood. The rapid clearance continued until 30 min postinjection when only 6% ID/g was left in the blood.

We subsequently determined the tissue distribution of [^{64}Cu]7 by sacrificing the mice at 24 h p.i. immediately after microPET/CT scans. Tumor, organs, and tissues of interest were excised and weighed; the radioactivity of harvested tissues was measured using γ-counter (Perkin-Elmer Packard, CT). The decay-corrected %ID/g of organs and tumors are shown in Table 1.

Table 1. Decay-Corrected Biodistribution of [^{64}Cu]7 with or without Co-Injection of CUDC-101 in MDA-MB-231 Tumor Bearing Mice 24 h after Injection (n = 3)[a]

tissue	[^{64}Cu]7	[^{64}Cu]7 + CUDC-101
blood	0.50 ± 0.07	0.56 ± 0.26
heart	1.07 ± 0.01	1.09 ± 0.17
lung	1.51 ± 0.14	1.54 ± 0.41
liver	3.23 ± 1.25	2.51 ± 0.53
spleen	0.88 ± 0.35	0.99 ± 0.14
kidney	1.90 ± 0.06	1.69 ± 0.32
tumor	2.21 ± 0.18	1.36 ± 0.23
muscle	0.23 ± 0.02	0.24 ± 0.06
GI	0.75 ± 0.40	0.84 ± 0.26
tumor-to-normal tissue uptake ratio		
tumor/muscle	9.61 ± 1.54	5.70 ± 0.48
tumor/blood	4.44 ± 0.88	2.64 ± 0.83

[a]The data percentage of the injected dose per gram of tissue (%ID/g) except tumor-to-muscle ratio. Values are quoted as mean ± standard deviation (SD).

The biodistribution result demonstrated that the tumor uptake of [^{64}Cu]7 reached 2.21 ± 0.19%ID/g at 24 h p.i. in the imaging group, whereas the presence of nonradioactive CUDC-101 significantly reduced the tumor uptake to 1.36 ± 0.23% ID/g (P < 0.01) in the blocking group with a 38% decrease. For the imaging group (nonblocking), 3.23 ± 1.25% ID/g and 1.90 ± 0.06% ID/g remained in the liver and kidneys, respectively. The overall uptake of [^{64}Cu]7 in other tissues and organs of blocking group was similar to that of the nonblocking group. On the basis of the biodistribution results, the contrast ratio of tumor to muscle for the imaging groups was calculated as 9.61 ± 1.53, which made tumors clearly visible at 24 hs p.i. as shown in Figure 3a. Meanwhile, the corresponding value for the blocking group was 5.70 ± 0.48 with a 38% decrease. These data proved the HDAC specific binding of [^{64}Cu]7 in vivo. The biodistribution results were consistent with the quantitative analysis of microPET imaging.

In conclusion, we reported, to our knowledge, the first ^{64}Cu labeled probe [^{64}Cu]7 for PET imaging of HDACs in vivo using a triple-negative breast cancer xenograph model. From the enzymatic assay, the IC_{50} of this compound to HDACs was shown to be in the nanomolar range, which indicated the remaining HDAC activity during structure modification from HDAC inhibitor CUDC-101. The specific binding of radiolabeled probe [^{64}Cu]7 to HDACs was proven by the competition of [^{64}Cu]7 with increasing concentration of CUDC-101 using MDA-MB-231 breast cancer cells. MicroPET/CT imaging revealed rapid and high [^{64}Cu]7 uptake in MDA-MB-231 breast tumors, and HDAC specificity in vivo was also confirmed by blocking experiments. This proof-of-concept research demonstrated the feasibility of using small molecule HDAC inhibitor for HDAC imaging probe development. Further optimization of [^{64}Cu]7 by using different Cu chelators to achieve better distribution and tumor uptake will be performed in a following study. The success of HDAC specific imaging in breast cancer using [^{64}Cu]7 has potential to be translated in clinical applications to noninvasively document

dx.doi.org/10.1021/ml400191z | ACS Med. Chem. Lett. 2013, 4, 858−862

tumor HDAC status, select the right patients for HDAC targeted treatment, and monitor treatment efficacy.

■ ASSOCIATED CONTENT

Supporting Information

Full experimental details for compounds synthesized, procedures for radiolabeling, description of enzymatic and cell based assays, biodistribution and small animal PET imaging studies. This material is available free of charge via the Internet at http://pubs.acs.org.

■ AUTHOR INFORMATION

Corresponding Author

*(Z.L.) Tel: +1 713-441-7962. Fax: +1 713-790-3018. E-mail: zli@tmhs.org.

Author Contributions

The manuscript was written through contributions of all authors. All authors have given approval to the final version of the manuscript.

Funding

This research was funded (or supported) by The Methodist Hospital Research Institute.

Notes

The authors declare no competing financial interest.

■ ABBREVIATIONS

HDAC, histone deacetylase; HDACi, histone deacetylase inhibitor; SAHA, suberoylanilide hydroxamic acid; ER, estrogen receptor; HER2, human epidermal growth factor receptor 2; PET, positron emission tomography; FAHA, [^{18}F]-fluoroacetamide)-1-hexanoicanilide; DOTA, 1,4,7,10-tetraazacyclododecane-1,4,7,10-tetraacetic acid; ROI, region-of-interest

■ REFERENCES

(1) Bolden, J. E.; Peart, M. J.; Johnstone, R. W. Anticancer activities of histone deacetylase inhibitors. *Nat. Rev. Drug Discovery* **2006**, *5* (9), 769−784.

(2) Minucci, S.; Pelicci, P. G. Histone deacetylase inhibitors and the promise of epigenetic (and more) treatments for cancer. *Nat. Rev. Cancer* **2006**, *6* (1), 38−51.

(3) Haberland, M.; Montgomery, R. L.; Olson, E. N. The many roles of histone deacetylases in development and physiology: implications for disease and therapy. *Nat. Rev. Genet.* **2009**, *10* (1), 32−42.

(4) Gregoretti, I. V.; Lee, Y. M.; Goodson, H. V. Molecular evolution of the histone deacetylase family: functional implications of phylogenetic analysis. *J. Mol. Biol.* **2004**, *338* (1), 17−31.

(5) de Ruijter, A. J.; van Gennip, A. H.; Caron, H. N.; Kemp, S.; van Kuilenburg, A. B. Histone deacetylases (HDACs): characterization of the classical HDAC family. *Biochem. J.* **2003**, *370* (Pt 3), 737−749.

(6) Weichert, W.; Roske, A.; Gekeler, V.; Beckers, T.; Stephan, C.; Jung, K.; Fritzsche, F. R.; Niesporek, S.; Denkert, C.; Dietel, M.; Kristiansen, G. Histone deacetylases 1, 2 and 3 are highly expressed in prostate cancer and HDAC2 expression is associated with shorter PSA relapse time after radical prostatectomy. *Br. J. Cancer* **2008**, *98* (3), 604−610.

(7) Weichert, W.; Roske, A.; Niesporek, S.; Noske, A.; Buckendahl, A. C.; Dietel, M.; Gekeler, V.; Boehm, M.; Beckers, T.; Denkert, C. Class I histone deacetylase expression has independent prognostic impact in human colorectal cancer: specific role of class I histone deacetylases in vitro and in vivo. *Clin. Cancer Res.* **2008**, *14* (6), 1669−1677.

(8) Rikimaru, T.; Taketomi, A.; Yamashita, Y.; Shirabe, K.; Hamatsu, T.; Shimada, M.; Maehara, Y. Clinical significance of histone deacetylase 1 expression in patients with hepatocellular carcinoma. *Oncology* **2007**, *72* (1−2), 69−74.

(9) Lane, A. A.; Chabner, B. A. Histone deacetylase inhibitors in cancer therapy. *J. Clin. Oncol.* **2009**, *27* (32), 5459−5468.

(10) Ropero, S.; Esteller, M. The role of histone deacetylases (HDACs) in human cancer. *Mol. Oncol.* **2007**, *1* (1), 19−25.

(11) Dokmanovic, M.; Clarke, C.; Marks, P. A. Histone deacetylase inhibitors: overview and perspectives. *Mol. Cancer Res.* **2007**, *5* (10), 981−989.

(12) Arrowsmith, C. H.; Bountra, C.; Fish, P. V.; Lee, K.; Schapira, M. Epigenetic protein families: a new frontier for drug discovery. *Nat. Rev. Drug Discovery* **2012**, *11* (5), 384−400.

(13) Jiaguo, H.; Zhiguo, L.; Wenbin, Z. Molecular probing and imaging of histone deacetylase inhibitors in cancer treatment. *Anticancer Agents Med. Chem.* **2012**, *12* (3), 182−186.

(14) Reid, A. E.; Hooker, J.; Shumay, E.; Logan, J.; Shea, C.; Kim, S. W.; Collins, S.; Xu, Y.; Volkow, N.; Fowler, J. S. Evaluation of 6-([(18)F]fluoroacetamido)-1-hexanoicanilide for PET imaging of histone deacetylase in the baboon brain. *Nucl. Med. Biol.* **2009**, *36* (3), 247−258.

(15) Hooker, J. M.; Kim, S. W.; Alexoff, D.; Xu, Y.; Shea, C.; Reid, A.; Volkow, N.; Fowler, J. S. Histone deacetylase inhibitor, MS-275, exhibits poor brain penetration: PK studies of [C]MS-275 using positron emission tomography. *ACS Chem. Neurosci.* **2010**, *1* (1), 65−73.

(16) Hendricks, J. A.; Keliher, E. J.; Marinelli, B.; Reiner, T.; Weissleder, R.; Mazitschek, R. In vivo PET imaging of histone deacetylases by 18F-suberoylanilide hydroxamic acid (18F-SAHA). *J. Med. Chem.* **2011**, *54* (15), 5576−5582.

(17) Krusche, C. A.; Wulfing, P.; Kersting, C.; Vloet, A.; Bocker, W.; Kiesel, L.; Beier, H. M.; Alfer, J. Histone deacetylase-1 and -3 protein expression in human breast cancer: A tissue microarray analysis. *Breast Cancer Res. Treat.* **2005**, *90* (1), 15−23.

(18) Zhang, Z.; Yamashita, H.; Toyama, T.; Sugiura, H.; Ando, Y.; Mita, K.; Hamaguchi, M.; Hara, Y.; Kobayashi, S.; Iwase, H. Quantitation of HDAC1 mRNA expression in invasive carcinoma of the breast. *Breast Cancer Res. Treat* **2005**, *94* (1), 11−16.

(19) Thurn, K. T.; Thomas, S.; Moore, A.; Munster, P. N. Rational therapeutic combinations with histone deacetylase inhibitors for the treatment of cancer. *Future Oncol.* **2011**, *7* (2), 263−283.

(20) Tate, C. R.; Rhodes, L. V.; Segar, H. C.; Driver, J. L.; Pounder, F. N.; Burow, M. E.; Collins-Burow, B. M. Targeting triple-negative breast cancer cells with the histone deacetylase inhibitor panobinostat. *Breast Cancer Res.* **2012**, *14* (3), R79.

(21) Sekar, T. V.; Dhanabalan, A.; Paulmurugan, R. Imaging cellular receptors in breast cancers: an overview. *Curr. Pharm. Biotechnol.* **2011**, *12* (4), 508−527.

(22) Cai, X.; Zhai, H. X.; Wang, J.; Forrester, J.; Qu, H.; Yin, L.; Lai, C. J.; Bao, R.; Qian, C. Discovery of 7-(4-(3-ethynylphenylamino)-7-methoxyquinazolin-6-yloxy)-*N*-hydroxyheptanamide (CUDC-101) as a potent multi-acting HDAC, EGFR, and HER2 inhibitor for the treatment of cancer. *J. Med. Chem.* **2010**, *53* (5), 2000−2009.

(23) Lai, C. J.; Bao, R.; Tao, X.; Wang, J.; Atoyan, R.; Qu, H.; Wang, D. G.; Yin, L.; Samson, M.; Forrester, J.; Zifcak, B.; Xu, G. X.; DellaRocca, S.; Zhai, H. X.; Cai, X.; Munger, W. E.; Keegan, M.; Pepicelli, C. V.; Qian, C. CUDC-101, a multitargeted inhibitor of histone deacetylase, epidermal growth factor receptor, and human epidermal growth factor receptor 2, exerts potent anticancer activity. *Cancer Res.* **2010**, *70* (9), 3647−3656.

(24) Salmi-Smail, C.; Fabre, A.; Dequiedt, F.; Restouin, A.; Castellano, R.; Garbit, S.; Roche, P.; Morelli, X.; Brunel, J. M.; Collette, Y. Modified cap group suberoylanilide hydroxamic acid histone deacetylase inhibitor derivatives reveal improved selective antileukemic activity. *J. Med. Chem.* **2010**, *53* (8), 3038−3047.

(25) Finnin, M. S.; Donigian, J. R.; Cohen, A.; Richon, V. M.; Rifkind, R. A.; Marks, P. A.; Breslow, R.; Pavletich, N. P. Structures of a histone deacetylase homologue bound to the TSA and SAHA inhibitors. *Nature* **1999**, *401* (6749), 188−193.

(26) Nielsen, T. K.; Hildmann, C.; Dickmanns, A.; Schwienhorst, A.; Ficner, R. Crystal structure of a bacterial class 2 histone deacetylase homologue. *J. Mol. Biol.* **2005**, *354* (1), 107−120.

(27) Feng, W.; Lu, Z.; Luo, R. Z.; Zhang, X.; Seto, E.; Liao, W. S.; Yu, Y. Multiple histone deacetylases repress tumor suppressor gene ARHI in breast cancer. *Int. J. Cancer* **2007**, *120* (8), 1664−1668.